

# Crossmodal Matching Transformer for Interventional in TEVAR

MENG LI and CHANGYAN LIN\*, Beijing Anzhen Hospital, Capital Medical University; Beijing Key Laboratory of Fundamental Research on Biomechanics in Clinical Application; Beijing Institute of Heart, Lung & Blood Vessel Diseases;, China

LIXIA SHU†, Beijing Anzhen Hospital, Capital Medical University; Beijing Key Laboratory of Fundamental Research on Biomechanics in Clinical Application; Beijing Institute of Heart, Lung & Blood Vessel Diseases, China

XIN PU, Beijing Anzhen Hospital, Capital Medical University, China

YI CHEN, Beijing Anzhen Hospital, Capital Medical University, China

HENG WU, Beijing Anzhen Hospital, Capital Medical University, China

JIASONG LI, Beijing Anzhen Hospital, Capital Medical University, China

HONGSHUAI CAO, Beijing Anzhen Hospital, Capital Medical University, China

Since the mapping relationship between definitized intra-interventional 2D X-ray and undefined pre-interventional 3D Computed Tomography(CT) is uncertain, auxiliary positioning devices or body markers, such as medical implants, are commonly used to determine this relationship. However, such approaches can not be widely used in clinical due to the complex realities. To determine the mapping relationship, and achieve a initialization post estimation of human body without auxiliary equipment or markers, a cross-modal matching transformer network is proposed to matching 2D X-ray and 3D CT images directly. The proposed approach first deep learns skeletal features from 2D X-ray and 3D CT images. The features are then converted into 1D X-ray and CT representation vectors, which are combined using a multi-modal transformer. As a result, the well-trained network can directly predict the spatial correspondence between arbitrary 2D X-ray and 3D CT. The experimental results show that when combining our approach with the conventional approach, the achieved accuracy and speed can meet the basic clinical intervention needs, and it provides a new direction for intra-interventional registration.

CCS Concepts: • **Computing methodologies** → **Image processing**; **Neural networks**; • **Applied computing** → **Life and medical sciences**.

Additional Key Words and Phrases: transformer, crossmodal, registration, intervention

## ACM Reference Format:

Meng Li, Changyan Lin, Lixia Shu, Xin Pu, Yi Chen, Heng Wu, Jiasong Li, and Hongshuai Cao. 2021. Crossmodal Matching Transformer for Interventional in TEVAR. In *2021 6th International Conference on Biomedical Signal and Image Processing, August 20-22, 2021, Suzhou, China*. ACM, New York, NY, USA, 9 pages.

\*Corresponding author

†Corresponding author

Permission to make digital or hard copies of all or part of this work for personal or classroom use is granted without fee provided that copies are not made or distributed for profit or commercial advantage and that copies bear this notice and the full citation on the first page. Copyrights for components of this work owned by others than ACM must be honored. Abstracting with credit is permitted. To copy otherwise, or republish, to post on servers or to redistribute to lists, requires prior specific permission and/or a fee. Request permissions from [permissions@acm.org](mailto:permissions@acm.org).

*Suzhou, August 20-22, 2021, Suzhou, China*

© 2021 Association for Computing Machinery.

ACM ISBN 978-1-4503-9050-7.

## 1 INTRODUCTION

Thoracic Endovascular Aortic Repair (TEVAR) is the preferred treatment for thoracic aortic dilatation diseases as it allows the low mortality and complications [12]. Interventional therapy is often performed on two-dimensional(2D) medical images such as X-ray. Due to the lack of clear development of vessels under X-ray fluoroscopy, contrast agents which often cause serious complications have to be used in interventional therapy. This paper presents a medical image registration approach based on transformer to accurately develop the aorta and its branches directly on X-ray fluoroscopy. Due to the position of aortic arch is fixed by the arterial ligament and three arterial branches, it is considered immobile in proposed approach. The feasibility of this idea will be validated in Section.4.2.

Machine learning-based medical image registration methods are mostly divided into two categories: optimization-based and learning-based approaches. Optimization-based conventional approaches project the 3D CT data to 2D virtual X-ray, according to a series of projection parameters. Then searching for the most similar image to the real X-ray iteratively and determining its spatial transformation parameters, which is difficult to meet the requirement of real-time registration suffer from extremely high computational cost and sensation of initial estimates[7]. Although the recent development of deep learning have been successfully applied to various medical applications [9, 13–15], such techniques have been barely used for 3D CT data to 2D virtual X-ray image registration. Even some works simply applied Convolutional Neural Networks (CNNs), autoencoder (AEs) or other network structures to conduct feature extraction[18, 22] or similarity measurement [1, 3], which direct predict the registration parameter, they haven't solve the problem of time-consuming of iteratively optimization. More importantly, considering the certainty of intra-interventional human position and the uncertainty of pre-interventional CT data acquisition position, researchers had to choose positioning from two perspectives[5, 8] or using traumatic markers like medical implants[8] to solve the problems. In other words, these methods are not widely used in clinic.

Since pre-interventional 3D CT can provide accurate anatomical information, this paper adopts 2D-3D image registration method, The aim is to establish a direct connection between 2D X-ray and 3D CT. The main ideas of proposed method are as follows: two segmentation networks been used to segment skeletal features from two dimension. Then the extracted features are put into the crossmodal matching transformer module to matching features of different dimensions. After the process of learning mapping relationships, we embed five positioning parameters available in interventional imaging equipment into our network to improved the ability of the network. The main contributions of our research are:

- We propose to end-to-end learn spatial correspondence between a pair of certain 2D X-ray image and arbitrary 3D CT image. The well-trained model can address initial 2D-3D pose estimation without projecting CT to generate a large number of virtual X-ray.
- The proposed approach can directly segment 2D and 3D images whose latent features are then used for 2D-3D image registration using the cross-modal transformer. This provide a solution for the precise localization in TEVAR under X-ray, and can potentially reduce the use of contrast agents and the exposure time under radiation.

## 2 RELATED WORKS

### 2.1 Learning-based medical image segmentation

Although image segmentation technology has been widely used in the field of medicine, the methods used in clinic are still limited. Medical images have abundant spatial information (such as complex texture structure), and the process of network downsampling is easy to lose these spatial information. Encoder-decoder networks with symmetric structures[10, 13]. can be better preserve

these spatial information. Using the same method, Cicek et al. replaced the two-dimensional convolution layer with the three-dimensional convolution layer to construct 3D U-Net, and realized the end-to-end processing of 3D CT[2]. Although deep learning have shown significant progress compared with conventional algorithms, the process of medical image tagging is time-consuming and labor-consuming, which limits the further development of deep learning algorithms in clinic. Researchers consider more diverse ways of using unlabeled data[19, 21], but such segmentation methods are not suitable for registration tasks that are extremely sensitive to spatial position.

### 2.2 Multimodal data fusion

It is a natural idea to fuse the same features extracted from two- and three-dimensional neural networks. S-PCNN[20] divides the source image into several blocks, then calculate the spatial frequency (SF) of the blocks as linking strength beta of the PCNN. It is used to extract the medical imageures find the best oscillation frequency graph (OFG) iteratively. Although combined the information of multi-modal images, the time-consuming of divided blocks and iteration is not allowed in real-time medical image registration. Parallel cross CNN (PCCNN) model[16] extracts two group features of CNN in parallel through a couple of deep CNN data transform flows. The information of two streams are fused together after the first fully connected layers in each stream. After the final Softmax regression, the 1024-dimensional image feature vector is classified and recognized. The method which introduced depthwise separable convolution combined with depthwise and pointwise convolution to replace the standard convolution as a basic convolution module[4], respectively applies the convolution in different channels, and applies a  $1 \times 1$  convolution to combine separate features generated by the depthwise convolution to reduce the complexity and computational cost of model. The method of fusing information of unaligned multimodal language sequences gives us enlightenment[17]. By the method of multimodal transformer, they address the above issues in an end-to-end manner without explicitly aligning the audio, language, vision.

## 3 METHODOLOGY

The entire network structure is shown in Fig.1. The proposed network consists of four modules: 2D skeleton extraction module, 3D skeleton extraction module, cross-modal transformer module, and parameter embedding module.

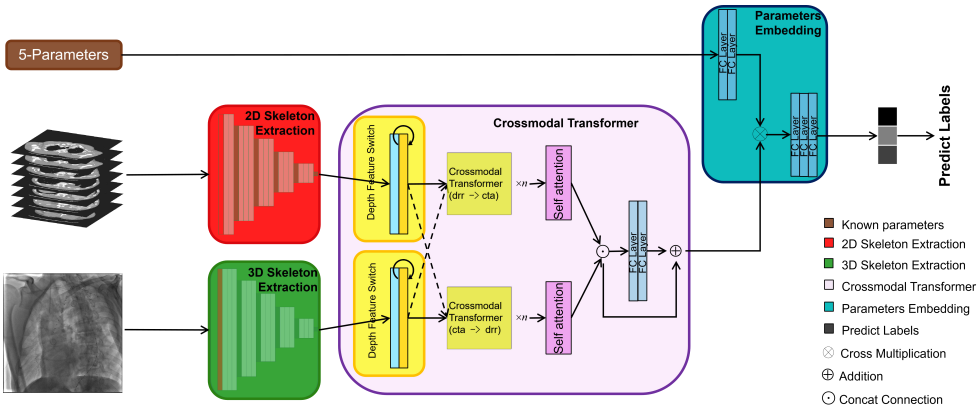


Fig. 1. The entire network structure of Crossmodal Transformer

### 3.1 Skeleton extraction

Our approach starts with extracting skeletons from 2D X-ray and 3D CT images. In particular, we train two UNet models for 2D skeleton segmentation and 3D skeleton segmentation tasks, as UNet has been successfully applied in various image segmentation tasks [2, 13]. After they are well trained, their encoders can consequently provide strong skeleton-related representations, and thus we take them as the input for downstream tasks.

As illustrated in Fig.2(a)(b), the 2D encoder is made up of five blocks that contains three 2D convolution units( a  $3 \times 3$  convolution layer, a batch normalization layer (BN) and a ReLU activation) and a  $3 \times 3$  max pooling layer with stride of two. Meanwhile, the 3D encoder is also made up of five blocks, where the first block has two 3D convolution units ( a  $3 \times 3 \times 3$  convolution layer, a batch normalization layer (BN) and a ReLU activation ) and a  $3 \times 3 \times 3$  max pooling with stride of two while Each of the rest four blocks containing three 3D convolution units and a 3D max pooling. In this paper, the output of the 2D and 3D encoder are 512-channel 2D feature maps and 64-channel 3D feature maps, representing the skeleton locations and appearance information of the 2D and 3D input.

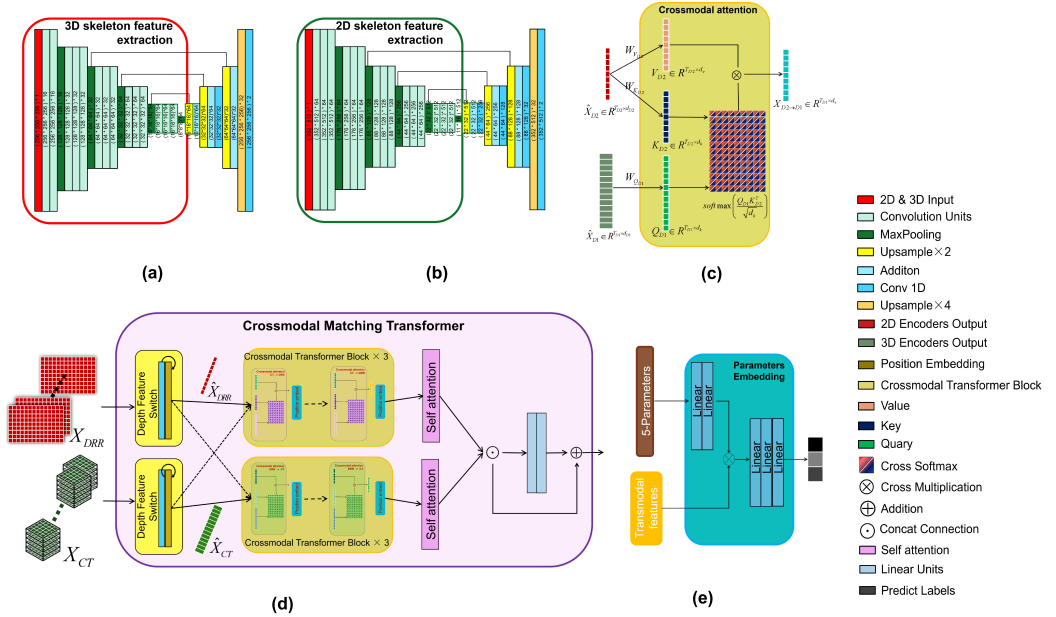


Fig. 2. Components of the network(a)(b)3D, 2D Skeleton Extraction Modules respectively;(c)Cross transformer block;(d)Cross-modal Matching Transformer Module;(e)Parameters Embedding Module;

### 3.2 Crossmodal matching transformer

After the feature extraction of 2D and 3D encoders, both of them are reshaped as a 1D vector for the multi-modal matching. This way, the 2D and 3D skeleton representations are directly combined for registration rather than previous approaches [6, 8] which convert 3D image to 2D then registration. The entire 2D-3D transformer module(Fig.2(d)) consists of two depth feature transform blocks, six cross-modal transformer blocks(Fig.2(c)), two self-attention blocks and two fully connected layers, which are explained as follows:

**3.2.1 Feature transform for semantic patch matching.** In the original extracted feature maps, each channel represents a unique type of feature that is extracted by a unique set of kernels comes from multiple convolution layers. Meanwhile, the same location of different feature maps correspond to the information that extracted from the same receptive field of the original data.

To better learn the relationship between the same semantic area of 3D CT and 2D X-ray data, we propose to transform original feature maps to a set of new feature maps, i.e., we re-organize a set of 2D feature maps of size  $N \times H \times W$  to a set of 1D feature maps of size  $S \times N$ , where  $S = H \times W$  or re-organize a set of 3D feature maps of size  $N \times H \times W \times L$  to a set of 1D feature maps of size  $S \times N$ , where  $S = H \times W \times L$ , where  $N$  represents the number of channels, and  $H, W, L$  denote the size of each feature map. After that, the transformed feature maps of both 2D and 3D data are flattened into 1D representations by  $1 \times 1$  temporal convolutional layer(1) using the following equation:

$$\hat{X}_D = Conv1D(X'_D, k_D, d) + PE(T_D, d) \quad (1)$$

This way, the position information of transformed feature maps is also embedded, i.e., it enables the 1D features to carry position information which is particularly important for 2D-3D image registration [17]. where  $T$  and  $d$  represent the feature length and dimension, respectively,  $k_D$  is the sizes of the convolutional kernels for modalities  $D$ ,  $d$  is the common dimension for adjustment.  $Conv1D(X'_D, k_D, d)$  and  $PE(T_D, d)$  represent dimension adjustment and position embedding, respectively.  $\hat{X}_D$  are the resulting different modalities feature with embedded position information.

**3.2.2 Crossmodal transformer block.** We then use the crossmodal transformer [17] for 3D and 2D representation fusion, where each crossmodal transformer block is combined with a multi-head crossmodal attention layer and a position embedding layer. The crossmodal attention layer could combine the information from the different sources of data. As shown in Fig.2(c), Querys, Keys, and Values has been defined as  $Q_{D1} = X_{D1} \times W_{Q_{D1}}, K_{D2} = X_{D2} \times W_{K_{D2}}, V_{D2} = X_{D2} \times W_{V_{D2}}$ , and with the weights of  $W_{Q_{D1}}, W_{K_{D2}}, W_{V_{D2}}$ . The matching from modality  $D1$  to  $D2$  can expressed as  $X_{D2 \rightarrow D1}$ .

Finally, the outputs of crossmodal transformer block are fed into a self-attention layer to enhance the registration performance based on both modalities.

### 3.3 Parameters embedding

Be different from the conventional six-degree-of-freedom(6-dof) based spatial transformations, all of the possible spatial transformations intra-interventional has been considered (Fig.3). It consist of eight parameters: the angle of L-arm rotation( $\alpha$ ), the angle of pivot rotation( $\beta$ ), the angle of C-arm rotation( $\gamma$ ), the distance from source to patient( $SSD$ ), the distance from source to detector( $SID$ ), and the coordinate of isocenter in pre-interventional CT data. Among these parameters, the first five could get from the imaging equipment and the last three are unknown parameters which should finally be predicted. Accuracy of geometric parameters derived from imaging equipment has been demonstrated in [11].

The parameters embedding module are shown in Fig.2(e). There are two fully connected layers that stretch 5 known parameters to 256 dimensions. The output are considered as the weight to restrict the matching features of the transformer. Finally, through last three fully connected layers, the three unknown labels are regressed.

## 4 EXPERIMENT RESULTS AND ANALYSIS

### 4.1 Implementation details

**4.1.1 Dataset.** Pre-interventional CT images of 1162 patients suffering thoracic aortic aneurysm or B aortic dissection were collected for training of 3D segmentation network. Among them, 1000 were used for training and 162 for validation. A total of 49176 frames of X-ray examination parameters

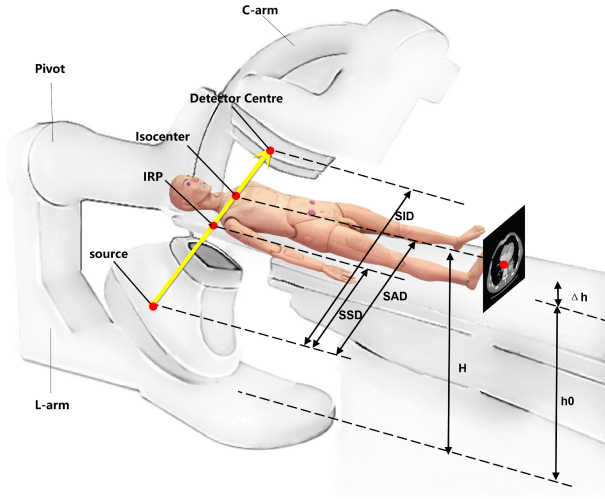


Fig. 3. C-arm and its parameters for positioning

were counted in 162 patients. Their distribution is shown in Fig.4. According to the distribution range of the above parameters and random sampling of the position coordinates of isocenter in CT space, the clinical projection transformation space is constructed.

Virtual intra-interventional X-rays are generated by ray casting to CT data with known clinical spatial transformation parameters. The input to 2D segmentation network is a  $352 \times 512$  image with 1 channels, which is cut out from the upper part of virtual X-ray for removing the part of the diaphragm with larger motion. The corresponding skeleton label is segmented from CT data using the threshold method. After that, the 873 groups pre-interventional CT images are tracing to generate 87300 virtual X-rays according to the range shown in table.1 and distribution shown in Fig.4. where  $d$  represents the scanning diameter of CT data.

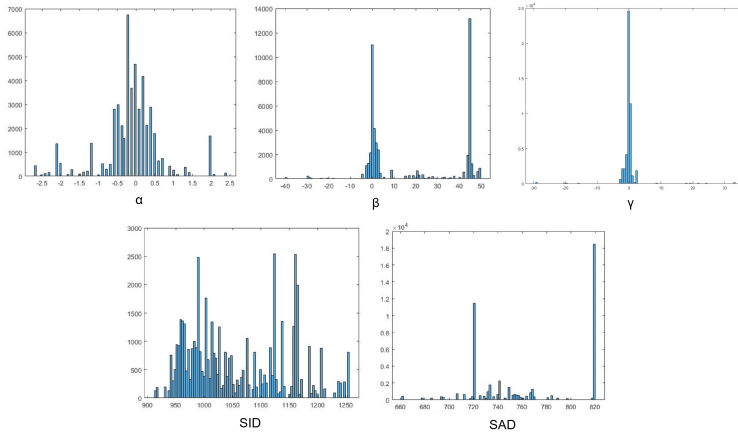


Fig. 4. Distribution of location-related parameters available from imaging equipment in TEVAR

Table 1. Transformation Space of Related Parameters

	$\alpha$	$\beta$	$\gamma$	$SID(mm)$	$SSD(mm)$	$Px(mm)$	$Py(mm)$	$Pz(mm)$
lower	$-2^\circ$	$0^\circ$	$-10^\circ$	850	720	300	$\tan \beta(Px - \frac{d}{2}) - 20$	170
upper	$2^\circ$	$50^\circ$	$10^\circ$	1250	820	480	$\tan \beta(Px - \frac{d}{2}) + 20$	210

**4.1.2 Training details.** We implement the proposed approach under the Pytorch framework with GPU acceleration. We first independently train two skeletal feature segmentation networks: 3D skeleton segmentation network was trained by 1000 sets of CT data and their skeletal labels and verified by 162 sets. And 2D skeleton segmentation network was trained by 543 groups virtual X-ray with a total of 543000 images and validated by 162 groups with a total of 97000 images. These virtual X-ray is generated according to the parameter distribution of clinical X-ray, as described in Section.4.1.1. For the optimization, 3D segmentation network use the stochastic gradient descent with 0.0001 initial learning rate and reduce the learning rate by half every 50 epoch, yet 2D segmentation network use Adam optimizing strategy with 0.0001 initial learning rate, which is empirical values obtained through training. After that, the down-sampling parameters of two trained segmentation networks are migrated to the Crossmodal Matching Transformer network to train the whole network.

## 4.2 Feasibility analysis of rigid registration to aortic arch

During interventional surgery, the doctor estimated the location of the branches of the aorta according to the position of the bone and the intraoperative guide wire under X-ray. In order to verify the rigid registration of bone can locate the aortic arch and its branches, we measured the displacement of vertebral bone, rib, guide wire and proximal stent in 309 groups intra-interventional X-ray. Because the vessel can not be clearly developed under X-ray, we use the displacement of the proximal stent post-interventional to approximate estimates the displacement of the aortic arch and its branches. As a validation of the feasibility of our method.

Table 2. The displacement of intra-interventional vertebral bone, rib, guide wire and post-interventional proximal stent

Object detected	Maximum( $mm$ )	Mean( $mm$ )
Guide wire	9.52	3.76
proximal stent	8.14	2.95
rib $0^\circ$	7.78	<b>0.78</b>
rib $45^\circ$	2.34	2.61
vertebral bone $0^\circ$	0.78	<b>0.31</b>
vertebral bone $45^\circ$	1.67	<b>0.91</b>

Since the average dynamic displacement error of branches vessels on aortic arch is about  $2.95mm$ , the opening diameter of the left subclavian artery is about 10 mm and the respect of proximal anchoring area over 15 mm, we have good reason to think that rigid registration can achieve the initial localization of the aorta in TEVAR.

### 4.3 Registration experiment

We compare our approach to a learning-based(CNN[8]) and two optimization-based methods. Cross-correlation(Opt-CC) and normalized mutual information(Opt-NMI) are used to measure the similarity respectively and Powell algorithm is used to optimize similarity iteratively. In addition, we compare the performance of the optimization-based approach using two learning-based approaches as initializers(Denoted as CNN+Opt and Cross-Transformer+Opt).

The position of the aortic branch on DSA image at same time is taken as the gold standard, and the registration error of these approaches(mean target registration error, mTRE) is measured. The gold standard data is untrained. The gross failure rate(GFR) is defined as the percentage of th tested cases with a TRE greater than  $10mm$ . And the average time cost of registration(Reg.time) and out-plane rotation error(Rot.error) additionally demonstrate of the superiority of the approach.

Table 3. Comparison of Registration Results

	GFR	Rot.error	mTRE(mm)	Reg.time(s)
Initial	90.48%	2.50°	17.68	-
Opt-CC	91%	2.58°	12.98	9.32
Opt-NMI	83%	2.70°	14.50	6.33
CNN	57%	3.13°	14.83	<b>0.85</b>
Cross-Transformer	17%	0°	<b>8.00</b>	<b>2.27</b>
CNN+Opt	0%	0.93°	<b>6.68</b>	4.73
Cross-Transformer+Opt	0%	0°	<b>4.70</b>	4.23

Experimental results in table 3 show that the accuracy and speed of registration are improved to some extent by using learning-based approach to initialize the optimization-based approach. The average displacement error of  $4.7mm$  is considered to be of clinical significance in TEVAR operation. Although this method is still not very robust in the comprehensive performance of registration, it is carried out without additional positioning equipment or markers.

## 5 CONCLUSION

In this paper, we propose a novel 3D-2D medical image registration approach. The main novelty of this paper is the proposed feature transform method that allows the generated feature maps retain the initial pose estimation of any 3D CT and corresponding 2D X-ray, without any other positioning items. Another novelty is we extended the crossmodal transformer to direct match 3D/2D data. The excellent experimental results shows that the proposed approach is suitable for basic clinical intervention usage and provides a new direction for intra-interventional registration.

Although deep learning has been widely used in the field of computer vision, its imprecision limits its application in the medical image registration. The approach of directly regression parameters is constrained by network performance, whose performance is not accurate enough to classify parameters. Pixel level accuracy is the most important problem to be solved in the field of registration. Other areas, such as image recognition, require translation rotation invariance, which is strictly prohibited in medical image registration. Therefore, the reference network structure should be more rigorous.

## 6 ACKNOWLEDGMENTS

Grant sponsor: Industry Quota of Beijing Public Welfare Research Institute;



## REFERENCES

- [1] Xi Cheng, Li Zhang, and Yefeng Zheng. 2018. Deep similarity learning for multimodal medical images. *Computer Methods in Biomechanics and Biomedical Engineering: Imaging & Visualization* 6, 3 (2018), 248–252.
- [2] Özgün Çiçek, Ahmed Abdulkadir, Soeren S Lienkamp, Thomas Brox, and Olaf Ronneberger. 2016. 3D U-Net: learning dense volumetric segmentation from sparse annotation. In *International conference on medical image computing and computer-assisted intervention*. Springer, 424–432.
- [3] Sayan Ghosal and Nilanjan Ray. 2017. Deep deformable registration: Enhancing accuracy by fully convolutional neural net. *Pattern Recognition Letters* 94 (2017), 81–86.
- [4] Guofa Li, Yifan Yang, Xingda Qu, Dongpu Cao, and Keqiang Li. 2020. A deep learning based image enhancement approach for autonomous driving at night. *Knowledge-Based Systems* (2020), 106617.
- [5] Haofu Liao, Wei-An Lin, Jiarui Zhang, Jingdan Zhang, Jiebo Luo, and S Kevin Zhou. 2019. Multiview 2D/3D rigid registration via a point-of-interest network for tracking and triangulation. In *Proceedings of the IEEE/CVF Conference on Computer Vision and Pattern Recognition*. 12638–12647.
- [6] Haofu Liao, Wei-An Lin, Jiarui Zhang, Jingdan Zhang, Jiebo Luo, and S Kevin Zhou. 2019. Multiview 2d/3d rigid registration via a point-of-interest network for tracking and triangulation. In *Proceedings of the IEEE Conference on Computer Vision and Pattern Recognition*. 12638–12647.
- [7] Stefan Matl, Richard Brosig, Maximilian Baust, Nassir Navab, and Stefanie Demirci. 2017. Vascular image registration techniques: A living review. *Medical image analysis* 35 (2017), 1–17.
- [8] Shun Miao, Sebastian Piat, Peter Fischer, Ahmet Tuysuzoglu, Philip Mewes, Tommaso Mansi, and Rui Liao. 2018. Dilated fcn for multi-agent 2d/3d medical image registration. In *Proceedings of the AAAI Conference on Artificial Intelligence*, Vol. 32.
- [9] Tulin Ozturk, Muhammed Talo, Eylul Azra Yildirim, Ulas Baran Baloglu, Ozal Yildirim, and U Rajendra Acharya. 2020. Automated detection of COVID-19 cases using deep neural networks with X-ray images. *Computers in biology and medicine* 121 (2020), 103792.
- [10] Tran Minh Quan, David GC Hildebrand, and Won-Ki Jeong. 2016. Fusionnet: A deep fully residual convolutional neural network for image segmentation in connectomics. *arXiv preprint arXiv:1612.05360* (2016).
- [11] Volker Rasche, B Schreiber, C Graeff, Thomas Istel, Hermann Schomberg, Michael Grass, Reiner Koppe, Erhard Klotz, and Georg Rose. 2003. Performance of image intensifier-equipped X-ray systems for three-dimensional imaging. In *International Congress Series*, Vol. 1256. Elsevier, 187–192.
- [12] Adnan Z Rizvi, M Hassan Murad, Ronald M Fairman, Patricia J Erwin, and Victor M Montori. 2009. The effect of left subclavian artery coverage on morbidity and mortality in patients undergoing endovascular thoracic aortic interventions: a systematic review and meta-analysis. *Journal of vascular surgery* 50, 5 (2009), 1159–1169.
- [13] Olaf Ronneberger, Philipp Fischer, and Thomas Brox. 2015. U-net: Convolutional networks for biomedical image segmentation. In *International Conference on Medical image computing and computer-assisted intervention*. Springer, 234–241.
- [14] Siyang Song, Shashank Jaiswal, Linlin Shen, and Michel Valstar. 2020. Spectral representation of behaviour primitives for depression analysis. *IEEE Transactions on Affective Computing* (2020).
- [15] Siyang Song, Linlin Shen, and Michel Valstar. 2018. Human behaviour-based automatic depression analysis using hand-crafted statistics and deep learned spectral features. In *2018 13th IEEE International Conference on Automatic Face & Gesture Recognition (FG 2018)*. IEEE, 158–165.
- [16] PJ Tang, HL Wang, and LX Zuo. 2016. Parallel cross deep convolution neural networks model. *Journal of Image and Graphics* 21, 3 (2016), 339–347.
- [17] Yao-Hung Hubert Tsai, Shaojie Bai, Paul Pu Liang, J Zico Kolter, Louis-Philippe Morency, and Ruslan Salakhutdinov. 2019. Multimodal transformer for unaligned multimodal language sequences. In *Proceedings of the conference. Association for Computational Linguistics. Meeting*, Vol. 2019. NIH Public Access, 6558.
- [18] Guorong Wu, Minjeong Kim, Qian Wang, Brent C Munsell, and Dinggang Shen. 2015. Scalable high-performance image registration framework by unsupervised deep feature representations learning. *IEEE Transactions on Biomedical Engineering* 63, 7 (2015), 1505–1516.
- [19] Kun Xu, Hang Su, Jun Zhu, Ji-Song Guan, and Bo Zhang. 2016. Neuron segmentation based on CNN with semi-supervised regularization. In *Proceedings of the IEEE conference on computer vision and pattern recognition workshops*. 20–28.
- [20] Hengfen Yang, Xin Jin, and Dongming Zhou. 2015. Block medical image fusion based on adaptive PCNN. In *2015 6th IEEE International Conference on Software Engineering and Service Science (ICSESS)*. IEEE, 330–333.
- [21] Xin Yi, Ekta Walia, and Paul Babyn. 2019. Generative adversarial network in medical imaging: A review. *Medical image analysis* 58 (2019), 101552.
- [22] Liya Zhao and Kebin Jia. 2015. Deep adaptive log-demons: diffeomorphic image registration with very large deformations. *Computational and Mathematical Methods in Medicine* 2015 (2015).